J. Fluid Mech. (1976), *vol.* 75, *part* 2, *pp.* 373–383
Printed in Great Britain

Experimental investigation of shock waves in liquid helium I and II

By JOHN C. CUMMINGS

Graduate Aeronautical Laboratories, California Institute of Technology, Pasadena†

(Received 19 August 1975)

The flow field produced by a shock wave reflecting from a helium gas–liquid interface was investigated using a cryogenic shock tube. Incident and reflected shock waves were observed in the gas; transmitted first- and second-sound shocks were observed in the liquid. Wave diagrams are constructed to compare the data with theoretical wave trajectories. Qualitative agreement between data and theory is shown. Quantitative differences between data and theory indicate a need for further analysis of both the gas–liquid interface and the propagation of nonlinear waves in liquid helium.

This work was a first step in the experimental investigation of a complex non-equilibrium state. The results demonstrate clearly the usefulness of the cryogenic shock tube as a research tool. The well-controlled jump in temperature and pressure across the incident shock wave provides unique initial conditions for the study of dynamic phenomena in superfluid helium.

1. Introduction

Helium is the only element that can exist as a liquid at 0 °K. At a temperature of 2·17 °K, helium experiences a λ-transition from liquid helium I (LHe I) to liquid helium II (LHe II). The fluid mechanics of LHe I do not differ qualitatively from those of an ordinary fluid. LHe II, on the other hand, is a superfluid demonstrating quantum effects on a macroscopic scale. Considerable work has been done on the fluid mechanics of LHe, but very little in the range where nonlinear effects are dominant or even important (see, for example, Putterman 1974). The present work is the first step in an investigation of shock waves in LHe, in particular of shock waves in LHe II.

Finite-amplitude first- and second-sound waves

The well-known two-fluid model (London 1938*a*, *b*; Landau 1941) explains many of the unusual properties of LHe II. This model assumes that the liquid is composed of a superfluid and a normal fluid that can move relative to one another without transferring momentum or energy. In LHe II, both pressure and temperature perturbations propagate as waves, and hence two types of shock wave exist: one a pressure shock with little temperature change, the other a temperature

† Present address: Division 5262, Sandia Laboratories, Albequerque, New Mexico 87115.

shock with little pressure change. The jump conditions for these shocks are easily derived from the two-fluid equations. These equations, plus the liquid equation of state, do not lend themselves to general analytical solution. Khalatnikov (1952, 1965) determined the governing equations for weak shock waves by retaining terms of order w^2 in the hydrodynamic equations, where $\mathbf{w} = \mathbf{v}_n - \mathbf{v}_s$ is the relative velocity between the normal fluid (subscript n) and the superfluid (subscript s).

For a pressure discontinuity Δp, Khalatnikov showed that

$$C_{10} = (\partial p/\partial \rho)^{\frac{1}{2}},$$

$$C_1 = C_{10}\left[1 + \frac{\Delta p}{2}\frac{\partial}{\partial p}\ln(\rho C_{10})\right]$$

and

$$v = \Delta p/\rho C_{10},$$

where C_{10} is the first-sound wave speed, C_1 is the first-sound shock speed, v is the particle velocity, p is the pressure and ρ is the density. He demonstrated that the temperature rise and relative velocity associated with a pressure wave are of third order in v/C_{10}.

For a temperature discontinuity ΔT, Khalatnikov found that

$$C_{20} = \left(\frac{\rho_s}{\rho_n}\frac{Ts^2}{C_h}\right)^{\frac{1}{2}},$$

$$C_2 = C_{20}\left[1 + \frac{\Delta T}{2}\frac{\partial}{\partial T}\ln\left(C_{20}^3\frac{\partial s}{\partial T}\right)\right]$$

and

$$w = \left[\frac{\rho}{\rho_n}\frac{s}{C_{20}}\right]\Delta T,$$

where C_{20} is the second-sound wave speed, C_2 is the second-sound shock speed, T is the temperature, s is the entropy per unit mass and C_h is the heat capacity per unit mass. The pressure rise and particle velocity associated with a temperature wave are of second order in w/C_{20}.

First- and second-sound shock waves

Osborne (1951) studied second-sound shock waves experimentally. This work was essentially qualitative, but many of the features of finite-amplitude second-sound waves were established. Dessler & Fairbank (1956) established the validity of Khalatnikov's analysis for $w/C_{20} \lesssim 10^{-2}$. Gulyaev (1969, 1970) published experimental results of optical studies of large-amplitude second sound. To the author's knowledge, there has been no experimental work on finite-amplitude first-sound waves in LHe.

The gas–liquid impedance match for sound propagation in helium is much better than for other gases, consequently the present experiment attempted to generate shock waves in LHe by reflecting a shock wave (in helium gas) from the liquid free surface. As an example, consider a strong shock (Mach 10) propagating through helium vapour with initial pressure 3 Torr and temperature 1·46 °K. The shock reflects from the LHe surface in a time of the order of 3 ns; it raises the

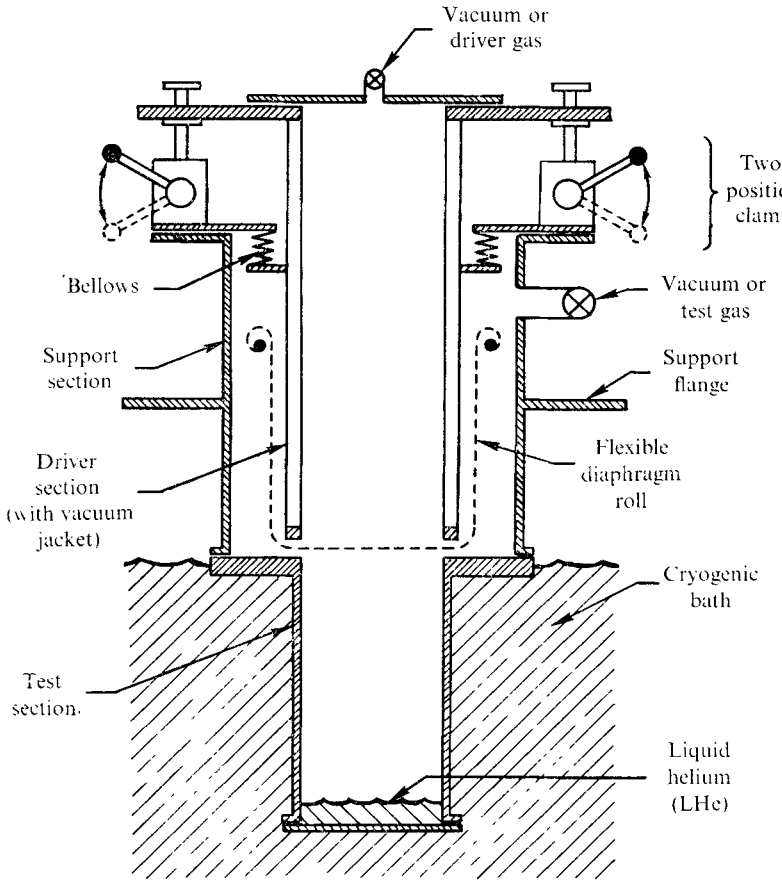

FIGURE 1. Schematic drawing of the cryogenic shock tube.

pressure to 2300 Torr and the gas temperature to 120 °K. Since LHe is highly compressible, this pressure jump creates a liquid particle velocity of 10 m/s and a first-sound shock wave which moves 13 % faster than the acoustic speed.† The sudden increase in gas temperature generates a second-sound shock wave in the liquid.

2. Experimental apparatus and procedure

The shock tube (figure 1) and cryogenic system have been previously described (Liepmann, Cummings & Rupert 1973) and discussed in detail (Cummings 1973, 1974). The shock tube was mounted vertically so that the test section could be immersed in a cryogenic bath. LHe condensed at the bottom of the test section (to a depth of roughly 2·5 cm) when helium gas was admitted to the shock tube.

Two types of instrumented lucite end walls (figure 2) were used on the end flange of the shock tube. The detectors in the gas used carbon card as the sensitive

† For a liquid, this is a very strong shock wave. A shock of comparable strength in water would be generated by a pressure jump of several thousand atmospheres.

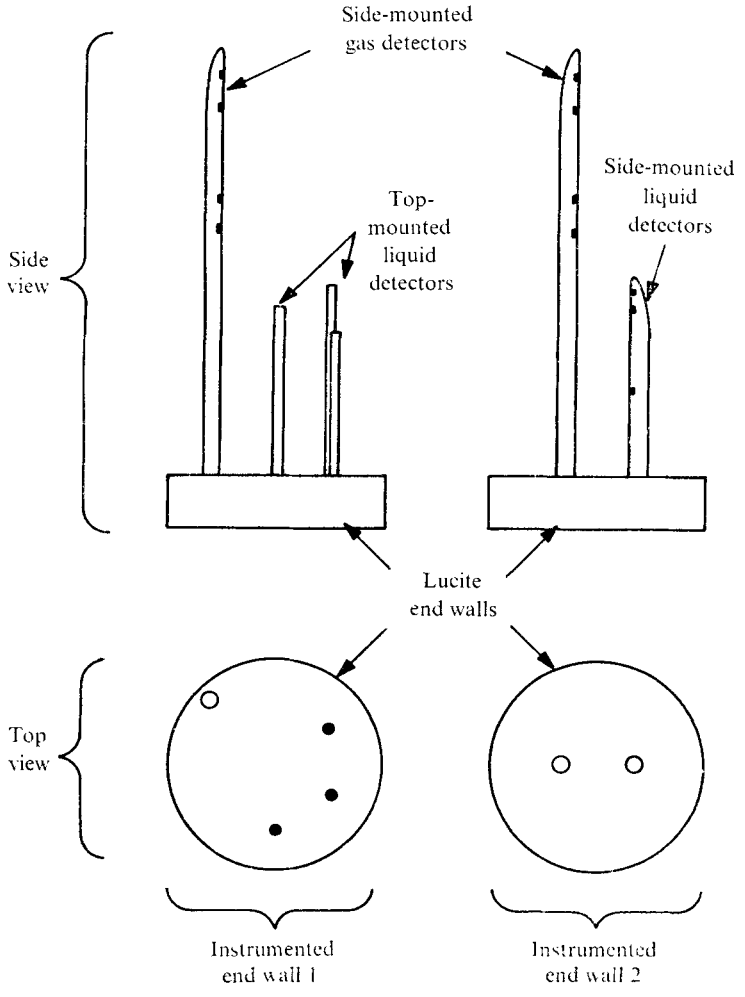

FIGURE 2. Instrumented end walls: gas and liquid detectors.

elements, while the detectors in the liquid employed flakes of carbon resistor. Most of the data were taken using the top-mounted liquid detectors. In this way, no wall or boundary-layer effects obscured the transmitted first- and second-sound signals. In addition, the signal levels were large because the waves reflected from the detectors.

To measure wave velocities and arrival times accurately, the top-mounted detectors depended on the shock waves reflecting off a plane liquid surface. The scatter in the data taken with these detectors indicated that the liquid surface was not absolutely plane over the cross-section of the shock tube. The side-mounted liquid detectors eliminated the dependence on a plane surface, thereby reducing the data scatter. A decreased signal level and increased rise time were the main disadvantages of these detectors.

A calibration cell (figure 3) was constructed for the purpose of dynamically calibrating the detectors in the liquid. The cell was a model of the shock-tube test

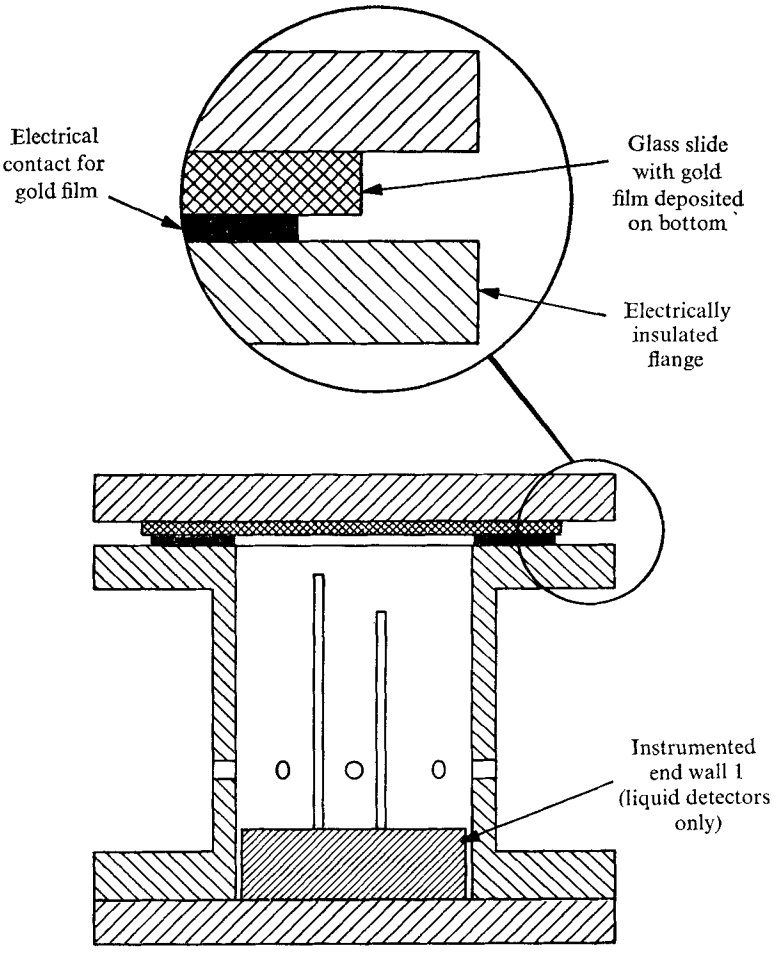

FIGURE 3. Schematic drawing of the calibration cell.

section with an electrical second-sound emitter in place of the liquid free surface. This emitter consisted of a gold film (roughly 100 Å thick) evaporated onto a glass slide. An electronic pulse generator was used to heat the emitter with a square-wave voltage pulse of adjustable amplitude and duration.

3. Results and discussion

Two parameters were varied: the test-gas pressure p_1 (and, therefore, the gas–liquid temperature) and the liquid depth. Helium gas at $\sim$ 300 °K and 30–35 psia was used as the driver gas for all runs. A series of tests was conducted for one LHe I condition:

$$p_1 = 47 \text{ Torr } (2{\cdot}26 \text{ °K}).$$

Four LHe II temperature cases were investigated:

$$p_1 = 25 \text{ Torr } (2{\cdot}02 \text{ °K}), \quad p_1 = 18 \text{ Torr } (1{\cdot}91 \text{ °K}),$$
$$p_1 = 9 \text{ Torr } (1{\cdot}71 \text{ °K}), \quad p_1 = 3 \text{ Torr } (1{\cdot}46 \text{ °K}).$$

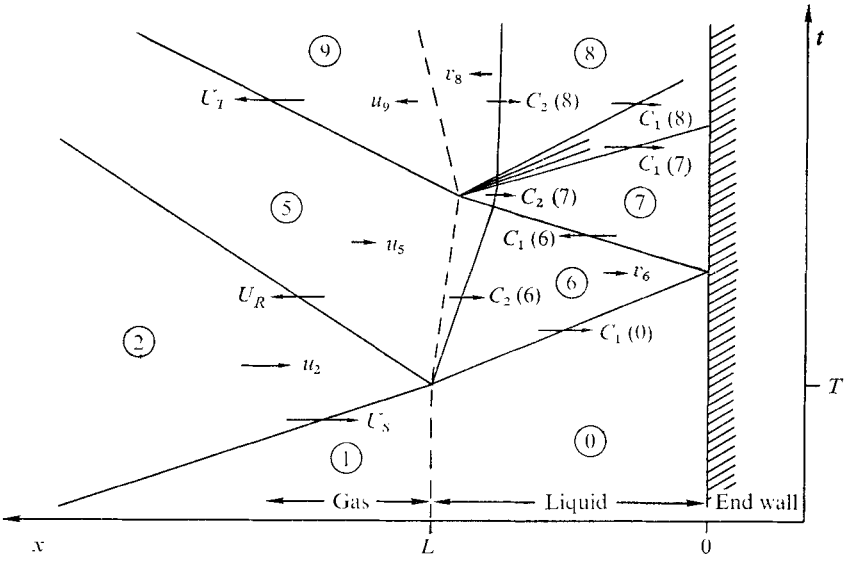

FIGURE 7. Schematic wave diagram: flow field and notation.

Typical oscillograms which show the arrival of the incident and reflected gasdynamic shocks, first-sound shock waves and second-sound shock waves are shown in figures 4, 5 and 6 (plates 1, 2 and 3) respectively. Using the oscillogram data, a wave diagram was constructed for each experimental run. The known location of each detector defined the spatial co-ordinate, and the temporal co-ordinate was determined from the oscillogram arrival times.

The complex nature of the gas–liquid flow field can be illustrated in a schematic wave diagram. Figure 7 shows the principal waves that are generated when a gasdynamic shock reflects from LHe II. In this figure, the gas–liquid interface is shown as a dashed line. The gas extends to the left from the line and the liquid to the right (confined by the lucite end wall at $x = 0$). The wave lines and notation that appear on figure 7 are defined as follows: incident shock wave, U_S; reflected shock wave, U_R; transmitted first-sound shock, $C_1(0)$; transmitted second-sound shock, $C_2(6)$, $C_2(7)$ and $C_2(8)$; transmitted shock wave, U_T; reflected first-sound shock, $C_1(6)$; rereflected first-sound wave, $C_1(7)$–$C_1(8)$; particle velocities, u_2, u_5, v_6, u_9 and v_8; initial liquid depth, L; arrival time of the incident shock, T.

χ, τ *diagrams*

In order to present all the data from one test-pressure case on a single wave diagram, it was necessary to use the following similarity parameters:

$$\chi \equiv (L-x)/L, \quad \tau \equiv (t-T)/L.$$

In the χ,τ plane, $\chi = 0$ represents the initial gas–liquid interface, $\chi = +1$ represents the lucite end wall, $\tau < 0$ refers to time before the shock reflects from the liquid, and $\tau > 0$ to time after the reflexion. Note that, while χ is dimensionless, τ has the dimensions of inverse velocity (μs/cm). The liquid depth L and the arrival time T of the shock wave at the liquid surface were

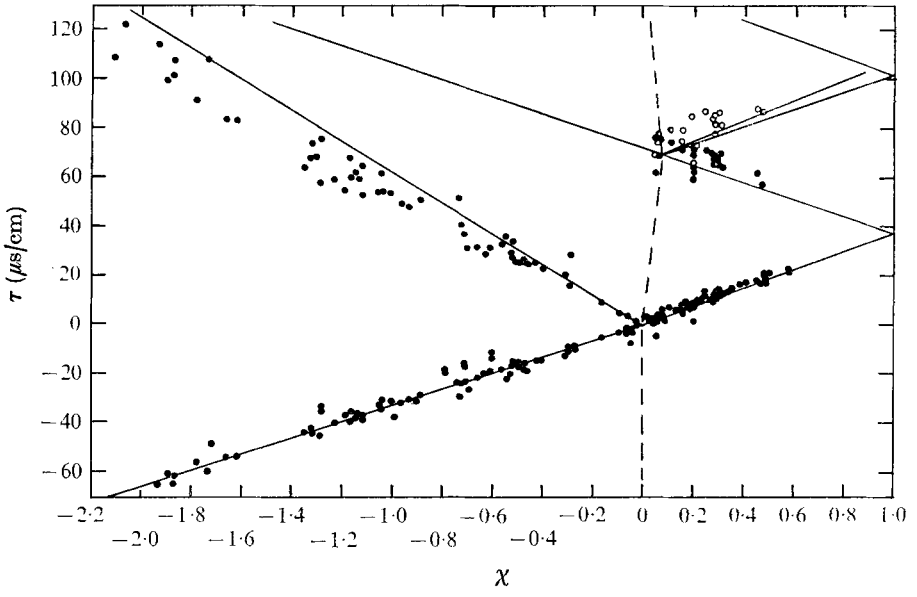

FIGURE 8. χ, τ diagram for $T_1 = T_0 = 2{\cdot}26$ °K (LHe I). ○, data from the rereflected first-sound wave.

calculated from the intersection of the wave lines corresponding to the incident shock, reflected shock, transmitted first-sound shock and transmitted second-sound shock. Using this method, the liquid level was determined to within ± 1 mm (the side-mounted liquid detectors determined L to $\pm 0{\cdot}5$ mm).

χ, τ diagrams for two of the experimental cases are shown in figures 8 and 9. For the LHe I case, figure 8, the liquid detectors were used to record the transmitted, reflected and rereflected first-sound shock waves. In the LHe II case, figure 9, these detectors monitored the transmitted first- and second-sound shock waves (the apparent arrival of the gas–liquid interface is shown for several runs using the side-mounted detectors).

All wave lines shown in the χ, τ diagrams are based on theoretical computations† (except the incident-shock lines, which were used as input for these computations). The gas flow field was calculated using the equations for an ideal gas and ideal shock tube. The first-sound shock waves were calculated using Khalatnikov's finite-amplitude theory. The velocities of second-sound shock waves are those of infinitesimal amplitude, corrected for the region pressure and added as vectors to the region particle velocity. Table 1 summarizes the calculated flow-field variables for all experimental cases.

The gas flow field

The incident shock wave. The observed incident-shock velocity was 82–92 % of that predicted using the equations for an ideal gas and ideal shock tube. This discrepancy may have been due to the finite distance for shock-wave formation

† A more detailed analysis may be found in Cummings (1973).

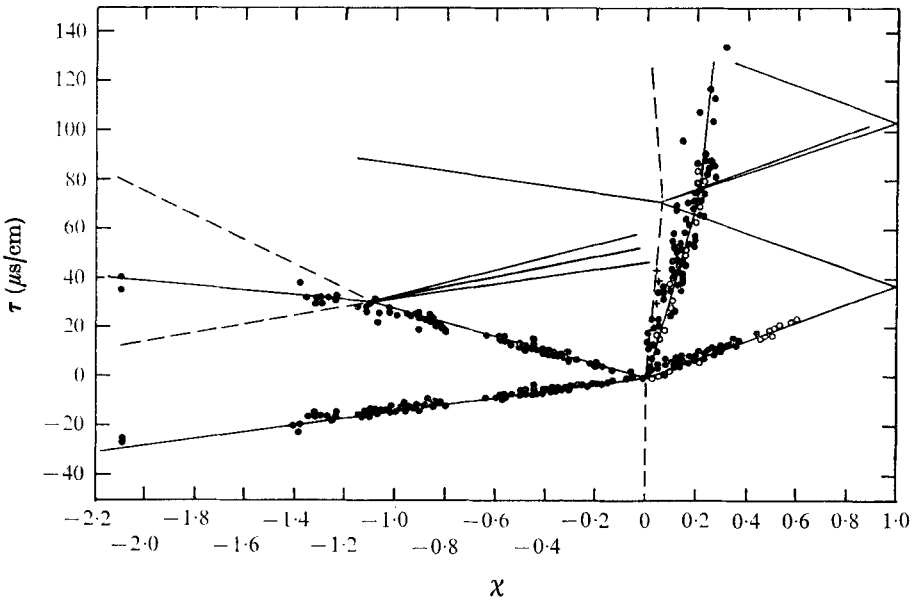

FIGURE 9. χ, τ diagram for $T_1 = T_0 = 1{\cdot}46$ °K (LHe II). ○, data from the side-mounted liquid detectors; +, apparent arrival of the gas–liquid interface.

$T_1 = T_0$	(°K)	2·26	2·02	1·91	1·71	1·46
$p_1 = p_0$	(Torr)	47	25	18	9	3
$p_5 = p_6$	(atm)	4·4	4·2	3·6	3·7	3·5
p_7	(atm)	9·4	8·9	7·6	7·8	7·4
$p_8 = p_9$	(atm)	5·0	4·6	3·9	4·0	3·7
T_2	(°K)	12	14	15	24	44
T_5	(°K)	24	32	35	57	120
U_R	(m/s)	160	184	198	248	361
U_T	(m/s)	290	334	348	447	648
u_2	(m/s)	220	269	299	406	562
$u_5 = v_6$	(m/s)	12·0	11·5	10·1	10·3	9·9
$v_8 = u_9$	(m/s)	9·6	9·6	8·6	9·0	8·9
$C_1(0)$	(m/s)	244	247	248	251	252
$C_1(6)$	(m/s)	265	265	262	266	265
$C_1(7)$	(m/s)	291	286	282	286	285
$C_1(8)$	(m/s)	251	252	250	254	255
$C_2(6)$	(m/s)	—	25·8	27·6	29·9	29·2
$C_2(7)$	(m/s)	—	~9	15·8	18·5	18·6
$C_2(8)$	(m/s)	—	~4	8·8	10·5	10·4

TABLE 1. Theoretical flow-field values (calculated with the observed $\overline{U}_S$)

(Cummings 1973). An interesting aspect of the experiment was the existence of an LHe film (roughly 200 Å thick) on the shock-tube walls. This film began to vaporize with the passage of the incident shock wave, and consequently acted as a mass source at the wall. This effect was opposite to that of the wall boundary layer in that it lengthened the test time.

The reflected shock wave. The reflected shock wave travelled at a velocity which was $\sim 15\,\%$ larger than that calculated from the observed velocity of the incident shock wave. This may have been due to the mass-source effect of vaporization at the LHe surface. Mass addition due to vaporization of the gas–liquid interface is similar to the mass-deletion effect of a thermal layer. When a shock wave reflects from a 'cold' end wall, the increased gas density at the wall acts like a receding piston and slows the reflected shock wave. This effect decays as $(t-T)^{-\frac{1}{2}}$. Sturtevant & Slachmuylders (1964) find that, when $R = U_R^2(t-T)/K_5$ is of the order of 10^3, the velocity of the reflected shock has returned to $\sim 96\,\%$ of the ideal value. For the cases considered here, $R = 10^3$ when $t-T = 100$ ns.

The physical processes that occur at the liquid free surface are very complex and are only qualitatively understood at this time. As the gasdynamic shock wave reflects from the liquid, the surface will begin to vaporize.† This vaporization will strengthen the reflected shock and the transmitted first-sound shock. For the LHe II cases, the region near the surface will likely contain LHe I that has been created dynamically by the large heat flux at the gas–liquid interface. A more detailed investigation of the gas–liquid interface using optical techniques is at present being conducted (Liepmann 1975, private communication).

The transmitted shock wave. A shock wave was transmitted to the gas when the first-sound wave reflected off the gas–liquid interface (figure 7). The velocity jump across this wave, $u_5 + u_9$, was small compared with the speed of sound in region 5. Therefore this shock was very weak and was not observed using the gas detectors.

The contact-surface arrival. The arrival of the contact surface can be seen in the diagrams only for the $p_1 = 3$ Torr case (figure 9). The interaction between the contact surface and reflected shock produced an expansion fan travelling into region 5. No experimental data were taken for this expansion fan.

The liquid flow field

The mean-free path of the test gas varied from $1{\cdot}8 \times 10^{-6}$ to $1{\cdot}8 \times 10^{-5}$ cm as p_1 varied from 47 to 3 Torr. For a shock wave that was 10 mean-free paths thick, the time of reflexion from the liquid surface varied from 1 to 3 ns. Consequently, the rise times of the transmitted first- and second-sound shocks were of the order of several nanoseconds.

First-sound shock waves. The observed first-sound shock speeds‡ were 2–7 % greater than those calculated using either the observed U_S values or the observed U_R values. The reason for this discrepancy is not clear. There may be higher-order terms in Khalatnikov's equation for C_1 which should be considered. It is also possible that surface vaporization provided an initial pressure pulse that was larger than that inferred from the U_R data.

The first-sound shock reflected off the lucite end wall and travelled back through the liquid. This reflected first-sound wave was a shock wave which

† A calculation of the gas–liquid interface temperature yielded values from 8 °K to 20 °K for the present cases.

‡ For a plane wave travelling through a *liquid*, the observed Mach numbers $M_1 = C_1/C_{10}$ were very large (M_1 varied from 1·10 to 1·13).

further compressed the liquid ($p_7 \doteq 2p_6$). When this wave reached the liquid surface, a rereflected expansion fan travelled back into the liquid, reducing the liquid pressure (a weak shock wave was transmitted into the gas). The reflected and rereflected first-sound waves can be readily observed in the LHe I case (see figure 5). The χ, τ diagram for this case (figure 8) shows qualitative agreement with the theoretical wave lines.

Second-sound shock waves. The second-sound velocities used in the χ, τ diagrams were computed as follows: the pressure and particle velocity in a region were calculated from the first-sound equations; the small-amplitude second-sound velocity for that pressure was then added as a vector to the particle velocity. Hence

$$C_2(6) = C_{20}(p_6, T_0) + v_6, \quad C_2(7) = C_{20}(p_7, T_0)$$

and

$$C_2(8) = C_{20}(p_8, T_0) - v_8.$$

The measured values of C_2 were generally 20–30 % greater than the small-amplitude values, but the data scatter was large. A more accurate measurement technique, employing superconducting thin-film gauges, is at present being used to determine the second-sound velocity (Laguna & Lidow 1974).

A comparison of signals generated by a shock wave and by the gold-film emitter is shown in figure 6 for a bath temperature of 1·46 °K. The received signal level in the calibration cell was roughly linear with the computed temperature rise.† Extrapolating the signal level to that produced in the shock tube (neglecting the effect of increased liquid pressure) yielded a value of $\Delta T \sim 45 \times 10^{-3}$ °K for the 1·46 °K case. At 1·71 °K and 1·91 °K, the shock tube ΔT was $\sim 50 \times 10^{-3}$ °K and $\sim 36 \times 10^{-3}$ °K, respectively. These values of ΔT correspond to a relative velocity† of approximately 3 m/s and hence $w/C_{20} \doteq 0{\cdot}15$.

4. Conclusions

A cryogenic shock tube was used to investigate the flow field produced by a shock wave that reflected from a helium gas–liquid interface. Wave diagrams have been constructed from the data: the incident, reflected and transmitted shock trajectories are shown. For LHe I, a single transmitted shock was observed in the liquid; for LHe II, two transmitted shocks (corresponding to first and second sound) were observed.

The wave trajectories and liquid flow field were computed using Khalatnikov's expressions for nonlinear first- and second-sound waves. The small, but consistent, differences between theory and experiment may be due to limitations of the second-order theory or to vaporization processes at the gas–liquid interface: both warrant further investigation.

These experiments demonstrate the feasibility of using shock waves to investigate nonlinear wave phenomena in liquid helium.

† Based on Khalatnikov's analysis.

This work was made possible by the U.S. Air Force Office of Scientific Research (Grant AFOSR 71-2092), and is based on Part II of a thesis submitted in partial fulfilment of the requirements for a Ph.D. degree at the California Institute of Technology. The author wishes to acknowledge the many contributions to this work that were made by Prof. Hans W. Liepmann.

REFERENCES

CUMMINGS, J. C. 1973 Ph.D. thesis, California Institute of Technology.

CUMMINGS, J. C. 1974 *J. Fluid Mech.* **66**, 177.

DESSLER, A. J. & FAIRBANK, W. M. 1956 *Phys. Rev.* **104**, 6.

GULYAEV, A. E. 1969 *Zh. Eksp. Theor. Fiz.* **57**, 59.

GULYAEV, A. E. 1970 *Zh. Eksp. Theor. Fiz. Pis. Red.* **11**, 332.

KHALATNIKOV, I. M. 1952 *Zh. Eksp. Theor. Fiz.* **23**, 253.

KHALATNIKOV, I. M. 1965 *Introduction to the Theory of Superfluidity* (trans. Pierre C. Hohenberg). New York: W. A. Benjamin Inc.

LAGUNA, G. & LIDOW, A. 1974 *Ann. Meeting Div. Fluid Dyn. Am. Phys. Soc., Pasadena, California*, paper SDC 1.

LANDAU, L. 1941 *J. Phys. U.S.S.R.* **5**, 71.

LIEPMANN, H. W., CUMMINGS, J. C. & RUPERT, V. C. 1973 *Phys. Fluids*, **16**, 332.

LONDON, F. 1938*a* *Nature*, **141**, 643.

LONDON, F. 1938*b* *Phys. Rev.* **54**, 947.

OSBORNE, D. V. 1951 *Proc. Phys. Soc. Lond.* A**64**, 114.

PUTTERMAN, S. J. 1974 *Superfluid Hydrodynamics*. North-Holland.

STURTEVANT, B. & SLACHMUYLDERS, E. 1964 *Phys. Fluids*, **7**, 1201.

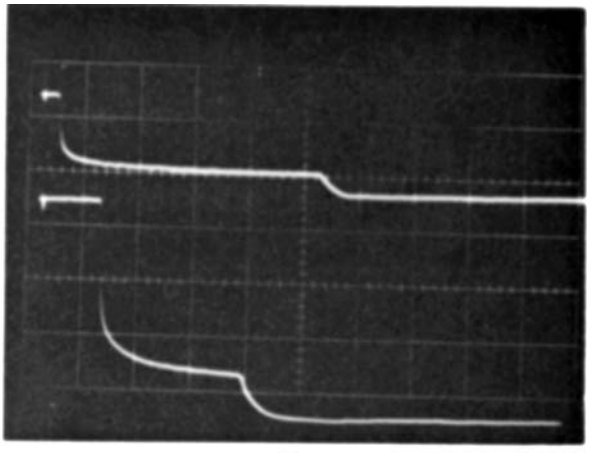

(*a*)

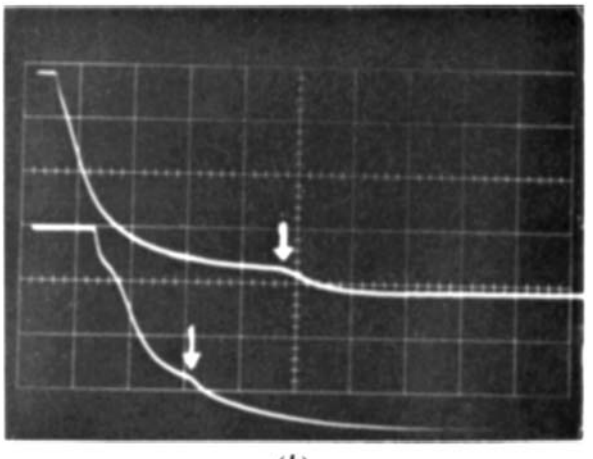

(*b*)

FIGURE 4. Response of the gas detectors to the incident and reflected shock. (*a*) $p_1 = p_0 = 47$ Torr, $T_1 = T_0 = 2{\cdot}26$ °K, 0·02 V/cm, 50 μs/cm. (*b*) $p_1 = p_0 = 3$ Torr, $T_1 = T_0 = 1{\cdot}46$ °K, 0·04 V/cm (upper beam), 0·03 V/cm (lower beam), 20 μs/cm.

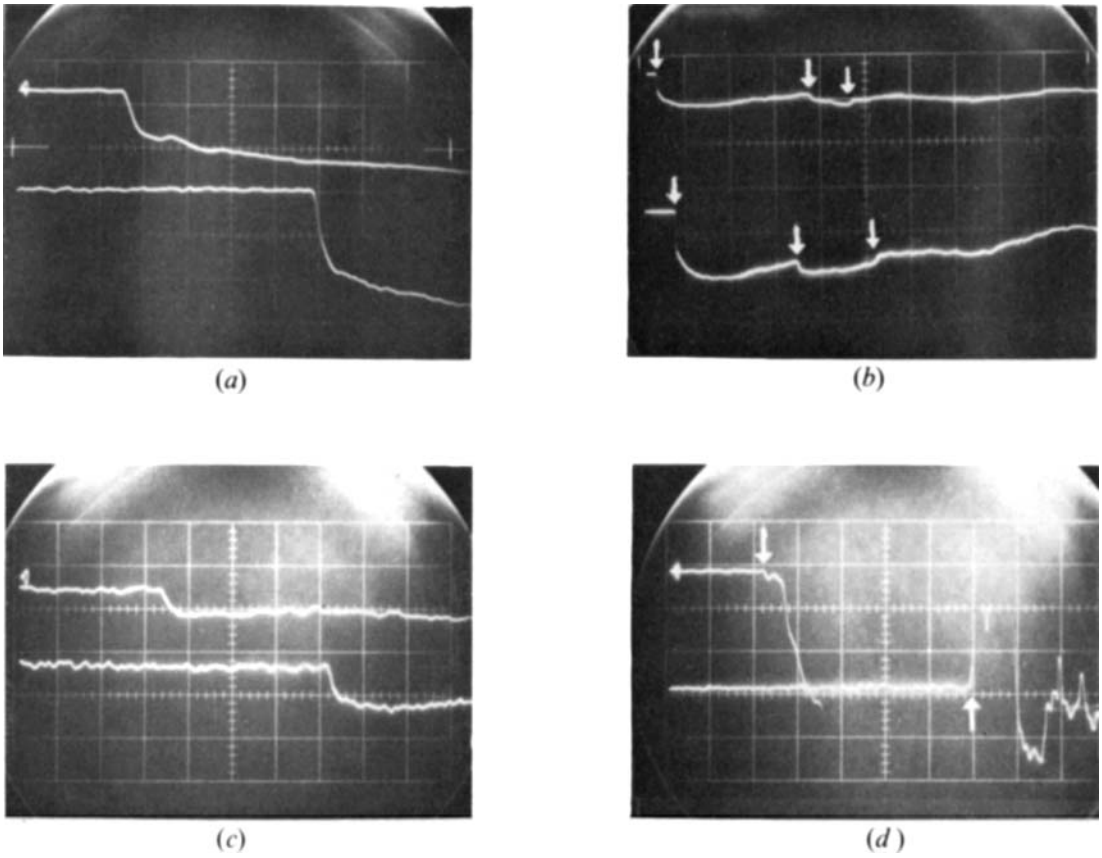

FIGURE 5. Response of the liquid detectors to the first-sound shock waves. (*a*) $p_1 = p_0 = 47$ Torr, $T_1 = T_0 = 2{\cdot}26$ °K, top-mounted detectors, 0·2 V/cm, 5 μs/cm. (*b*) $p_1 = p_0 = 47$ Torr, $T_1 = T_0 = 2{\cdot}26$ °K, top-mounted detectors, 0·5 V/cm, 50 μs/cm (transmitted, reflected, and rereflected waves). (*c*) $p_1 = p_0 = 3$ Torr, $T_1 = T_0 = 1{\cdot}46$ °K, top-mounted detectors, 0·05 V/cm, 5 μs/cm. (*d*) $p_1 = p_0 = 47$ Torr, $T_1 = T_0 = 2{\cdot}26$ °K, side-mounted detectors, 0·2 V/cm, 10 μs/cm.

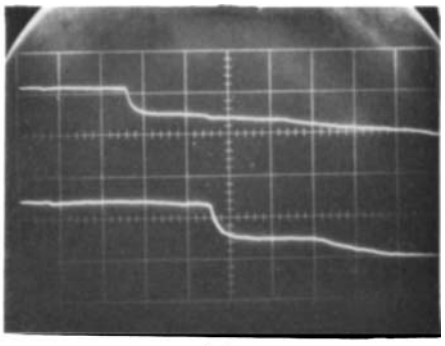

(*a*)

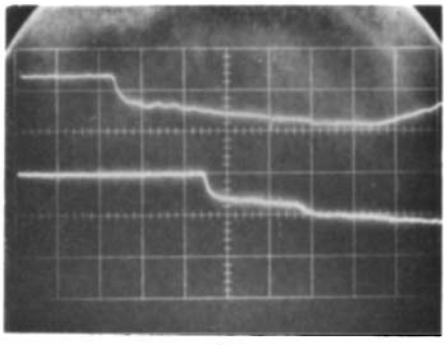

(*b*)

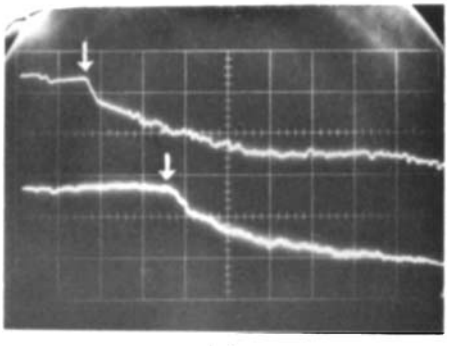

(*c*)

FIGURE 6. Response of the liquid detectors to second-sound shock waves: shock-tube and calibration-cell data ($T_1 = T_0 = 1{\cdot}46$ °K). (*a*) Top-mounted detectors, 0·5 V/cm, 50 μs/cm, data taken using shock tube. (*b*) Top-mounted detectors, 0·2 V/cm, 50 μs/cm, data taken using calibration cell. (*c*) Side-mounted detectors, 0·2 V/cm, 50 μs/cm, data taken using shock tube.